Available online at www.sciencedirect.com
ScienceDirect
Thermochimica Acta 461 (2007) 107–121
thermochimica acta
www.elsevier.com/locate/tca

High performance differential scanning calorimetry (HPer DSC): A powerful analytical tool for the study of the metastability of polymers

Geert Vanden Poel [a,*], Vincent B.F. Mathot [b]

[a] *DSM Resolve, P.O. Box 18, 6160 MD Geleen, The Netherlands*
[b] *SciTe, Ridder Vosstraat 6, 6162 AX Geleen, The Netherlands*

Available online 8 April 2007

Abstract

The crystallization and melting behavior of polypropylene (PP), polyoxymethylene (POM) and polyamide-6 (PA6) has been investigated by means of varying the cooling and heating rates using a high performance differential scanning calorimeter (HPer DSC). The influence of the sample mass and scan rate on thermal lag has been sorted out and the importance of making proper corrections is stressed. By varying the cooling rates from 5 to 250 °C/min in combination with one particular heating rate (10 and 300 °C/min have been used) reorganization and especially recrystallization effects in a PP sample have been examined. Recrystallization of the PP can be avoided by using a high heating rate (300 °C/min). The influence of incorporating a stabilizer acting as a comonomer in the POM chain on the kinetics of the crystallization and melting behavior is studied. The influence of the maximum heating temperature in the melt on crystallization of POM and of POM with stabilizer is investigated by self-seeding experiments using high heating and cooling rates. Furthermore, the melting behavior of PA6, where several transitions take place during heating which are up to now not fully understood, is discussed subsequent to cooling at 5–300 °C/min. Throughout it has been made clear that it is important to have the capability of applying proper combinations of low/high and cooling/heating rates in order to examine the metastability of polymer systems and the related kinetics of transitions, to scrutinize the phenomena seen and to arrive at the right explanations.

Keywords: High performance differential scanning calorimeter (HPer DSC); HyperDSC™; Standard DSC; Cooling rate; Heating rate; Fast scanning rate; High-speed calorimetry; Polypropylene; Polyoxymethylene; Polyamide; Crystallization; Cold crystallization; Melting; Reorganization; Recrystallization

1. Introduction

1.1. Metastability

All steps: the constitution of a polymer during polymerization, the subsequent processing and addition of additives or other materials, and the establishing of the final shape of the product, strongly influence crystallization and morphology of a crystallizable material on a nano- to micrometer scale level with implications for the look, feel, mechanical and other properties of a product on a macro-scale. During these steps many changes occur with respect to the morphology, which transformations are related to the intrinsic metastability of polymer materials: whatever their history, they are susceptible to change as function of temperature and time, mechanical treatment, etc. Besides the importance for product development as sketched, the scientific aspects of metastability and the kinetics related are very intriguing. As metastability has appreciable implications for the thermal properties of a polymer system and, vice versa, thermal analysis and calorimetry on polymers provide insight in the kinetics of phenomena related to metastability it is worthwhile to study metastability in detail by dynamic calorimetry. For that reason, the present report discusses the use of low- to high-speed DSC for the study of the metastability present in some well-known polymers – polypropylene (PP), polyoxymethylene (POM) and polyamide 6 (PA6) – with a special focus on cooling and subsequent heating at a variety of scan rates.

As has been remarked, investigation of polymer solidification during *cooling* by vitrification or crystallization under processing conditions is a necessary step in order to understand, e.g. the final polymer product properties. Especially for crystallizable

* Corresponding author. Tel.: +31 46 4761623; fax: +31 46 4761200.
E-mail addresses: geert.poel-vanden@dsm.com (G. Vanden Poel), vincent.mathot@scite.eu (V.B.F. Mathot).

0040-6031/$ – see front matter © 2007 Geert Vanden Poel. Published by Elsevier B.V. All rights reserved.
doi:10.1016/j.tca.2007.04.009

polymers the analysis of the relationships between processing conditions and morphology of the sample obtained is crucial in material characterization. The effective cooling rate during processing – which will in general be different for different parts (core, skin, etc.) of the processed product, e.g. by injection molding – has a dominating influence on the sample morphology and end properties.

In addition to understanding of crystallization by cooling it is of great fundamental interest to understand and interpret DSC *heating* curves with respect to thermal history and morphology. This is relevant for PP and POM because of the occurrence of reorganization and recrystallization during heating, but it is especially important in the case of polymorphous polymers like PA6, for which cold crystallization and multiple melting are commonly observed in DSC heating curves.

1.2. High performance DSC (HPer DSC)

A relatively new version of high-speed calorimetry technology, high performance DSC (HPer DSC; see www.scite.eu), has recently been discussed for practical use and since then marketed by Perkin-Elmer under the name HyperDSC™, see www.hyperdsc.com. Mathot et al. published the detailed characteristics and use of this new mode of measurement, which represents a major step forward in high-speed calorimetry as compared to Standard DSC [1–3]. Controlled and constant scan rates of hundreds of degrees per minute and combinations thereof both in cooling and heating are enabled. Heats of transition, heat capacities, temperature-dependent crystallinities, etc., can be established at the extreme rates applied. The short measuring times also enable the high throughput needed in combinatorial chemistry.

Application fields concerning HPer DSC are situated in the study of the kinetics and metastability of macromolecular and pharmaceutical systems, particularly in the analysis of rate-dependent phenomena at real temperature–time conditions. HPer DSC is very much suited to investigate kinetics of processes like crystallization, cold crystallization, recrystallization, annealing, and solid-state transformations in polymers, pharmaceuticals and liquid crystals. (Sub)milligram amounts of material can be investigated at controlled cooling and heating rates of hundreds of degrees per minute, which facilitates the analysis of films, expensive and extraordinary products, inhomogeneities in materials, etc. High cooling rates need to be applied to simulate processing conditions like in film blow molding, injection molding and extrusion. It turns out that for most processing techniques the cooling rate can be mimicked by HPer DSC. Measurements concerning metastability and kinetics of systems under study are also necessary to be able to (re)connect heating behavior with cooling history.

This article discusses the crystallization and melting behavior of several polymer materials studied by HPer DSC. Systematic studies by combining various cooling and heating rates, each of them strictly controlled by the HPer DSC, improve the understanding of the kinetics of processes like phase transitions, cold crystallization, recrystallization, and other reorganization effects in polymer materials.

2. Experimental

2.1. Experimental technique

Measurements were performed with a modified Perkin-Elmer Pyris 1 calorimeter having software version 9.0. This power-compensation DSC was selected to be used as an HPer DSC because its furnace has low mass and small dimensions, ensuring a much faster heat transfer than in existing commercial heat-flux calorimeters. The small gap between the furnace and the aluminum cooling system, which is even reduced by guard ring inserts, promotes effective cooling. The HPer DSC was cooled to a temperature of −178 °C with a cryofill liquid nitrogen cooling system, which provides a very effective heat sink. Special attention was paid to the avoidance of water uptake by the gas tubes in the instrument; to the cooling of the instrument electronics; and to the prevention of water vapor condensation. To prevent moisture in the system, a completely air-sealed glove box was installed on top of the HPer DSC. Dry nitrogen gas was used to purge the glove box. The choice of the gas atmosphere surrounding the reference and sample furnaces depends on the specific system and on the temperature range to be studied. In most cases, a mixture of 10% helium and 90% neon is suited for a combination of a temperature range of −176 to 585 °C and typical controlled, constant scan rates as high as 500 °C/min for the heating mode and 300 °C/min for the cooling mode (or even higher within a limited temperature range). Both inert gases do not condense under cooling by liquid nitrogen. With regard to the heat conduction to and from the reference and sample furnaces (the Pyris 1 DSC system features two small furnaces), the mixture offers a useful compromise [1,4]. Pure helium is in itself an excellent heat conductor and can be used to maximize heat transfer, which offers benefits in measurements down to very low (subambient) temperatures. However, when it comes to reaching high temperatures, the furnace will be a limiting factor, because the helium causes too much heat loss so that the furnace can no longer control the temperature beyond the ceiling level of about 200 °C. Neon [5] conducts heat less well (but better than nitrogen), and enables temperature control in the higher ranges. It is even possible to use standard nitrogen as long as it is prevented from condensing as a result of the presence of liquid nitrogen cooling. Default isothermal waiting times between runs amount to 5 min, although this time can be shortened to, e.g. 1 min. To promote optimal thermal contact between the sample and the sample container, a 15 μm thick, rectangular aluminum foil of approximately 0.5 cm × 1 cm is normally used to wrap the sample, instead of using a pan as sample container. On the reference holder an aluminum foil of the same dimensions and wrapped in the same way is placed. If a lower accuracy is acceptable, it is also possible to use aluminum pans.

2.2. Temperature calibration

In this article, an extensive temperature calibration of the HPer DSC has been applied in both heating and cooling mode for various sample masses and various rates according to the recommendations described in a previous article [2]. The

correct way to perform temperature calibration for the HPer DSC starts with a calibration as usual over a wide temperature range, with primary standards that are selected on the basis of their phase transition temperatures situated in the temperature range of interest. Adamantane, gallium, benzophenone, indium and tin have been used as primary standards to calibrate the Perkin-Elmer Pyris 1 in the heating mode for the temperature range from −150 up to 350 °C. The sample masses of these calibration substances were chosen in between 0.99 and 1.01 mg with an applied heating rate, S_h, of 10 °C/min.

Subsequent to the calibration of the HPer DSC two calibration matrices, one concerning the extrapolated onset and another concerning the peak temperature were constructed for various sample masses and for all heating rates applied. These values can be used to correct for the thermal lag of the extrapolated onset and the peak temperature of an HPer DSC curve, resulting from a measurement where a sample with a certain mass, m, has been scanned at a chosen heating rate, S_h, and also in case of a chosen cooling rate, S_c, see further on. Applying the right correction factor(s) is the only way to compare in a proper way the transition temperatures of a particular sample measured at various heating rates. It is important to understand that correcting the shape of the entire HPer DSC curve along the temperature axis is of no use because the thermal lag of each part of the curve depends in fact on the heat flow rate of that specific part, which is influenced by the amount of molecules taking part in the transition (like e.g. crystallization, melting, etc.) and in addition the sample mass and applied heating rate. Therefore, up to now no corrections have been made concerning the shape of the HPer DSC curves.

A separate calibration in the cooling mode is not necessary for the HPer DSC instrument used because the symmetry with respect to the cooling and heating modes is checked and found to be good [2].

3. Results and discussion

3.1. Polypropylene (PP)

3.1.1. Introduction

Polypropylene has been studied extensively and up-to-date information concerning molecular structure, processing, crystallization, melting and resulting morphology can be found in several textbooks [6–8,26].

Polypropylene is a thermoplastic polymer, which can be processed by means of virtually all thermoplastic-processing methods. It is used in a wide variety of applications, including food packaging, textiles, laboratory equipment, automotive components, and banknotes. As an addition polymer made from the monomer propylene, it is exceptionally resistant to many chemical solvents, bases and acids and also offers excellent electrical resistance. PP has very good resistance to fatigue, so that most plastic living hinges, such as those on flip-top bottles, are made from this material.

Most commercial PPs have a level of crystallinity intermediate between that of low density polyethylene (LDPE) and high density polyethylene (HDPE); their Young's moduli are also intermediate. Although it is less tough than LDPE, it is much less brittle than HDPE. This allows PP to be used increasingly as a replacement for engineering plastics, such as ABS. Interesting developments in this respect take place with respect to light-weight composites, by e.g. combining high-strength PP fibers in a PP matrix. Also for recycling reasons, current trends in the automotive sector are towards the development of 'all-PP' plastic parts.

PP usually melts around 160 °C. Food containers made from it will not melt in the dishwasher, and do not melt during industrial hot filling processes. For this reason, most plastic tubs for dairy products are made of PP sealed with aluminum foil (both heat-resistant materials).

Tacticity is an important structure parameter for understanding the link between molecular architecture and properties of PP. The orientation of each methyl group relative to the methyl groups of neighboring monomers has a strong effect on the polymer's ability to form crystals, because each methyl group takes up space while it constrains backbone bending.

Unlike most other vinyl polymers, useful PP grades have not been synthesized so far by radical polymerization. The material that results from such a process has methyl groups arranged randomly, leading to so-called atactic PP. The lack of ability to develop any long-range order prevents crystallinity in such a material, resulting in amorphous material with very little strength and few redeeming qualities.

A Ziegler–Natta catalyst is able to confine incoming monomers to a specific orientation, only adding them to the polymer chain if they face a right direction. Most commercially available PPs are made with titanium chloride catalysts, which produce predominantly isotactic PP. With the methyl group consistently on one side, segments of such molecules tend to turn into a helical shape; during subsequent cooling these helices can line up next to one another to form crystals that give commercial PP its strength.

More precisely engineered "Kaminsky" catalysts have been produced, which offer a much better level of control than Ziegler–Natta catalysts. Based on metallocene molecules, these catalysts use organic groups to control the monomers being added, so that properly chosen catalysts can produce isotactic, syndiotactic, or atactic PP, or even a combination of these. They also produce higher molar masses than traditional catalysts do, which can lead to further improvements of properties.

3.1.2. Results and discussion

To start with, specific heat capacity measurements (c_p) on the PP sample under investigation (melt flow rate at 230 °C and 2.16 kg = 2.0 g/10 min; density = 905 kg/m^3; medium isotacticity; broad molecular weight distribution), have been performed at a heating rate of 10 °C/min, using a Standard DSC. It illustrates that HPer DSC is not meant to replace Standard DSC, but should be seen as a complementary capability for researchers to apply *both* low and high heating rates, even using the same equipment. The heat capacity measurements were done according to the "continuous measuring method" [9]. Fig. 1 presents c_p measurements (using a Standard Perkin-Elmer DSC 7) of the PP in the cooling and the heating mode at a rate of 10 °C/min.

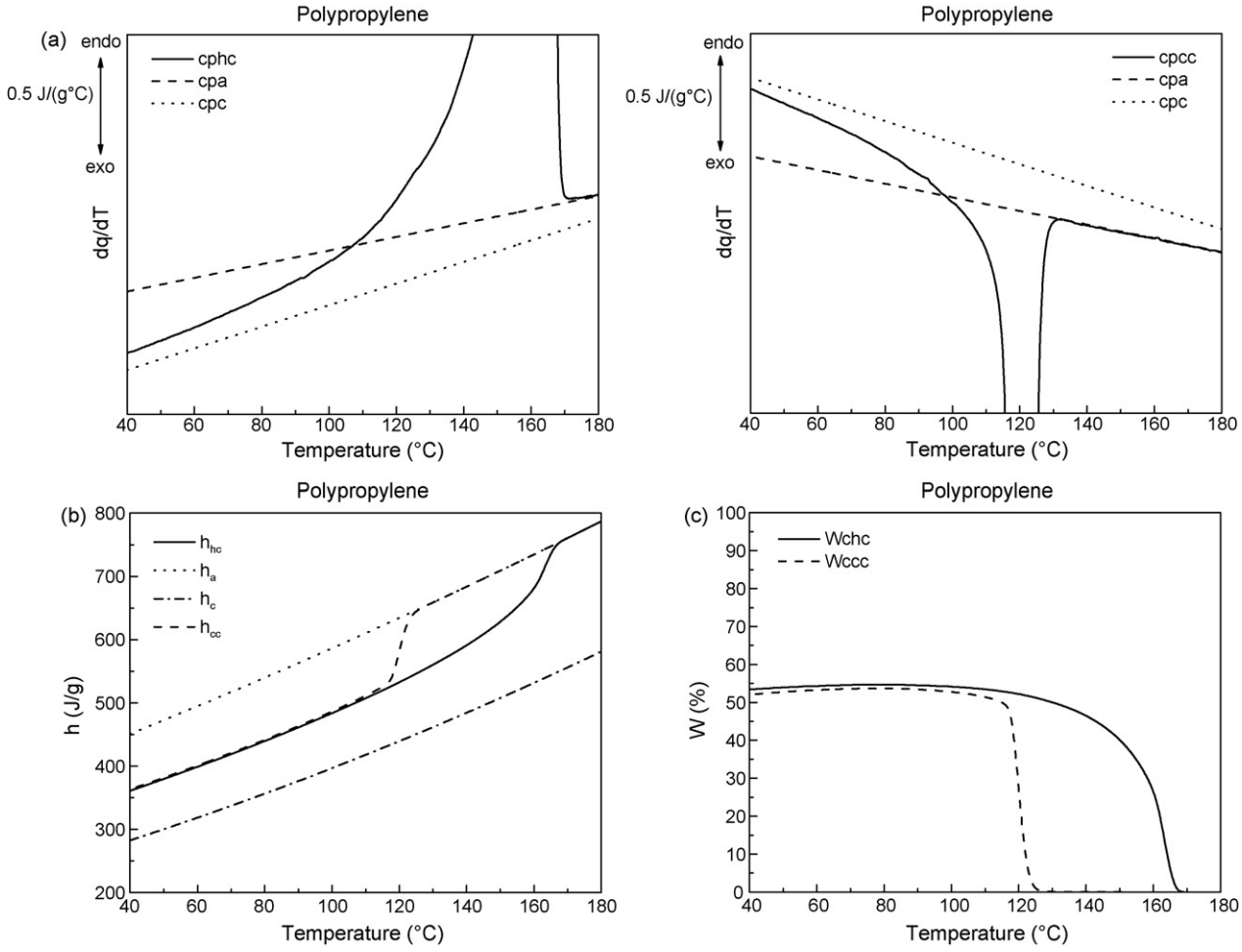

Fig. 1. Heat capacity measurements (a), and calculation of enthalpy (b) and crystallinity (c) curves in both cooling and heating at 10 °C/min for polypropylene.

In the figure, the c_p of PP is plotted as a function of temperature together with the heat capacity reference curves for 100% amorphous and 100% crystalline PP [10]. The enthalpies and crystallinities as function of temperature are additionally calculated [9] for this PP sample and plotted respectively in Fig. 1b and c, and it is seen that the crystallinity at low temperatures of the PP sample studied amounts to approximately 53%. Specific enthalpy cooling and heating curves h_{cc} and h_c respectively for a PP based on DSC-7 continuous heat capacity measurements and the reference curves h_c and h_a from ATHAS databank are presented in Fig. 1b. The enthalpy-based mass percentage crystallinity curves for cooling W_{ccc} and heating W_{chc} are shown in Fig. 1c.

The crystallization and melting behavior of PP has been investigated further using various cooling and heating rates. The cooling curves at various rates, from 5 up to 250 °C/min are plotted as a function of the temperature in Fig. 2, which curves are not corrected for the cooling rate. The curves, and by that the onset and peak temperatures, shift towards lower temperatures with increasing cooling rates as expected. The enthalpy of crystallization decreases with increasing cooling rate and by that also the crystallinity. The lowest cooling rates induce a rather narrow crystallization peak, while the highest cooling rates provoke broad crystallization curves. Though this broadening could be explained by the fast cooling rate overruling the increased overall crystallization rate (which is the result of the combined influence of increased nucleation and growth rates at increasing supercoolings), it could well be that also the temperature gradient within the sample is increasingly playing a role, see further on.

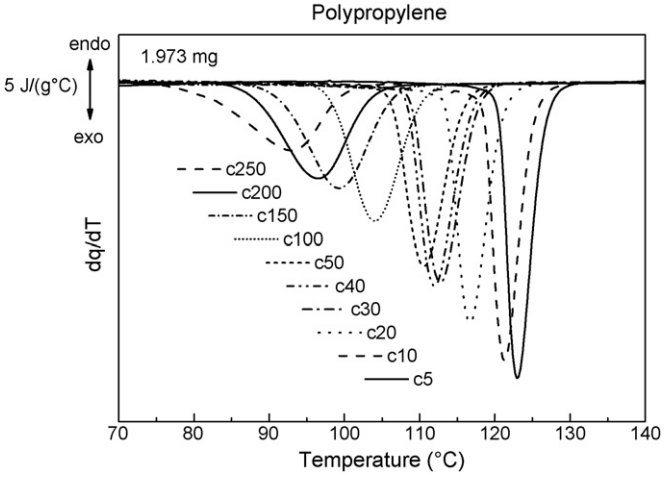

Fig. 2. Crystallization of PP at various cooling rates, not corrected for the cooling rate.

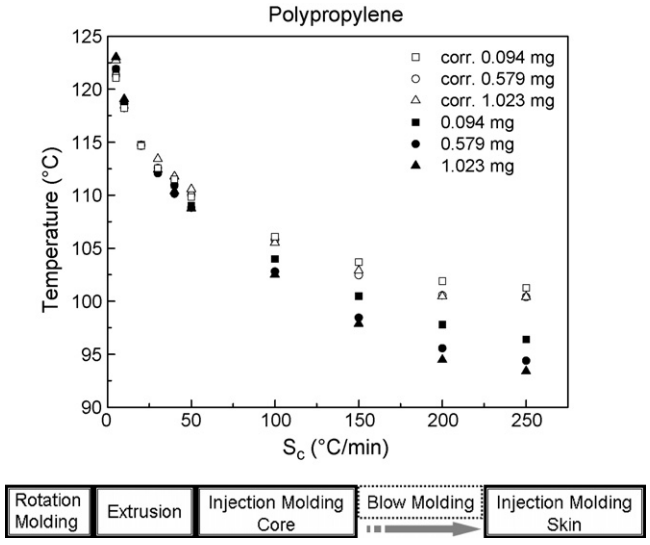

Fig. 3. Crystallization peak temperatures of PP samples having different masses as a function of cooling rate. Filled symbols: T_c values without correction. Open symbols: T_c values corrected for the sample mass and for the cooling rate applied.

The crystallization peak temperatures of PP samples having three different sample masses (m = 0.094, 0.579 and 1.023 mg) as a function of the cooling rate, S_c, are shown in Fig. 3. With increased, controlled cooling rates from 5 to 250 °C/min, the uncorrected crystallization peak temperatures of the PPs show a decrease of the crystallization temperatures of about maximal 30 °C. The 'real' crystallization peak temperatures of PP, i.e. the T_c values corrected for sample mass and cooling rate according to Table IV in Ref. [2], drop only maximal 25 °C. Controlled cooling rates of 300 °C/min can be achieved for samples with a very low mass (e.g. 0.094 mg), see the same figure. The uncorrected T_c values for the 1.023 mg sample are located somewhat beneath those of the 0.579 mg sample, especially at higher cooling rates. After applying the correction factor for peak temperature values, the T_c values of both samples coincide regardless of the sample mass. This result indicates the sample mass dependency and the importance to choose the right sample mass when using high cooling rates. One should carefully indicate the cooling history of the reported crystallization temperatures of polymers, and when comparing different crystallization temperatures, determined by various cooling rates, one has to take at least some correction factors (CF_{EO} and/or CF_P [2]) into account.

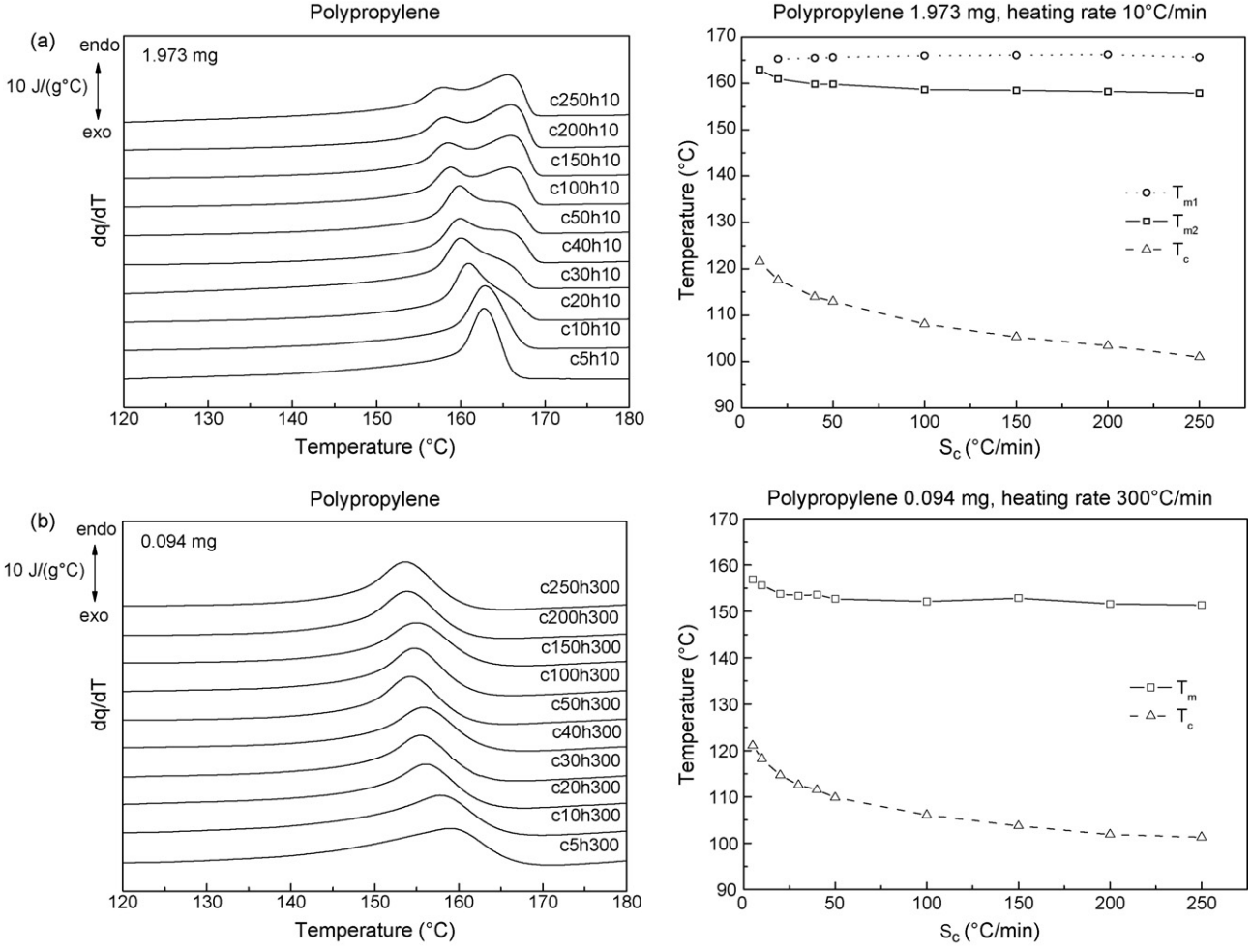

Fig. 4. (Left) HPer DSC heating curves of PP at (a) 10 °C/min and (b) corrected curves at 300 °C/min, subsequent to cooling rates at 5–250 °C/min. (Right) Characteristic temperatures (see text), corrected for sample mass, cooling rate and heating rate.

Thus, it is clear from the foregoing that corrections are needed in order to compare different temperature values obtained by changing the sample mass and various cooling and/or heating rates. For some experiments it is best to use different sample masses: e.g. a low sample mass, 0.1 mg, for very high cooling/heating rates (300 up to 500 °C/min) and a rather standard sample mass of about 1 mg for moderate cooling/heating rates (up to 150 °C/min). If the rates are not too far apart, experiments can be performed using just one, well-chosen sample mass simplifying the use of the correction factors.

Interesting enough, it is seen in Fig. 3 that the decreasing crystallization temperatures seems to level off at the highest cooling rates, which is quite unexpected, but also observed recently by others [11]. However, the decrease of T_c is still linear with the logarithmic of the increasing cooling rate, S_c. Nevertheless, it could indicate an increasing difficulty of the instrument with sample and container to realize the good thermal conductivities needed.

HPer DSC is capable to mimic the cooling rates of most processing techniques, like for instance rotation molding (about 5 up to 50 °C/min); extrusion (about 100 °C/min); the core of injection molding (about 50 up to 250 °C/min), etc.: all values being strongly dependent on the product dimensions (especially the thicknesses of its cross sections; the distances from core to skin, etc.) and the way of cooling by the mold. If there is a need to relate the properties of the (thin, outer part of a) skin of an injection molded product to the cooling rate exerted by the mold – in case of a very low mold-wall temperature – calorimetry using chip-technology [12–22] could be applied in addition.

Fig. 4 represents at the left-hand side HPer DSC curves of the PP melting at heating rates of 10 °C/min (Fig. 4a) and 300 °C/min (Fig. 4b) after applying controlled cooling rates from 5 up to 250 °C/min. The HPer DSC curves are corrected for the extrapolated onset values according to Table III in [2]. At the right-hand side, the characteristic peak temperature values – T_c, T_m, T_{m1} (the low-temperature melting peak), and T_{m2} (the high-temperature melting peak) – of PP are plotted as a function of the cooling rate, all corrected for sample mass, cooling rate and heating rate.

When no reorganization takes place, one expects the melting peak temperature to follow more or less the crystallization peak temperature with increasing preceding cooling rate. The lowest melting temperature, T_{m1}, in Fig. 4a however, follows the crystallization temperature only to a limited extent: the less lowering of T_{m1} compared to T_c is thought to be caused by extensive reorganization during heating, leading to increased perfection and/or increase in crystallite dimensions. The second, highest melting temperature, T_{m2}, remains more or less constant with increased preceding cooling rate, indicating it is caused by reorganization via recrystallization during the relatively slow heating at 10 °C/min. Such a second melting temperature typically arises when the applied heating rate is roughly lower than the preceding cooling rate used. Fig. 4b shows only one melting peak during fast heating at 300 °C/min after various preceding cooling rates and T_m follows the crystallization temperature again to a limited extent. In this case, the applied heating rate is for all cases equal to or higher than the cooling rate used. The rather high heating rate makes it possible to prevent reorganization by recrystallization, but it is not high enough to prevent the extensive reorganization effects during the melting, causing the lowest melting peak temperature to be higher than expected.

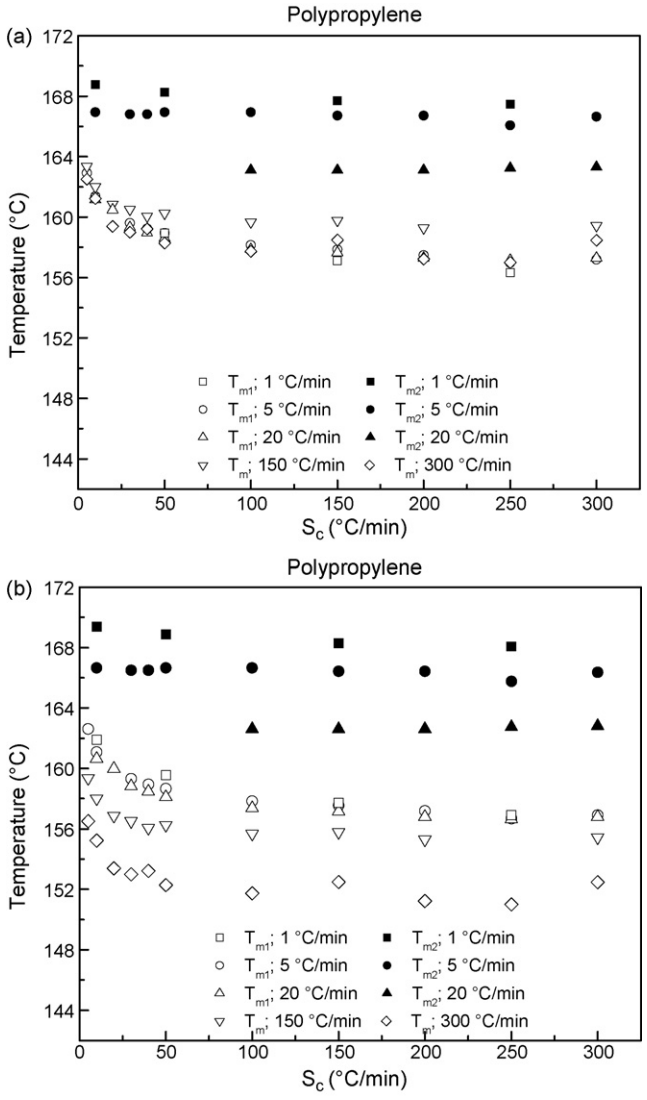

Fig. 5. The melting peak temperatures of PP at heating rates of 1, 5, 20, 150 and 300 °C/min subsequent to cooling at various rates (from 5 up to 300 °C/min): (a) uncorrected and (b) corrected for heating rate and sample mass.

The melting peak temperatures of PP at heating rates of 1, 5, 20, 150 and 300 °C/min subsequent to various cooling rates (from 5 up to 300 °C/min) are presented in Fig. 5. Without correction it is impossible to give a clear explanation of the results in Fig. 5a because different sample masses are used: 0.094 mg for the sample heated at 300 °C/min, 0.579 mg for the sample heated at 150 °C/min and 1.023 mg for the samples heated at 1, 5 and 20 °C/min. After correction according to the heating rate and sample mass (using the correction factors for the peak temperature, CF_P, in [2]) Fig. 5b presents the 'real' data, which can now be compared with each other. As is seen, two melting peak temperatures (T_{m1} and T_{m2}) are recorded for heating rates up to 5 °C/min. Heating at 20 °C/min partly suppresses recrystallization after cooling at rates up to 50 °C/min. From 40

onwards to 300 °C/min one single melting peak results, reflecting total suppression of recrystallization after all cooling rates applied. T_{m2}, reflecting melting of very stable crystals after recrystallization at the respective heating rate, is remarkably constant at low heating rates, irrespective of the preceding cooling rate. Because of the decreasing crystallization temperatures with increasing cooling rates, it reflects recrystallization in case fast cooling is followed by slow heating. In such cases, knowing already that these recrystallization effects can be avoided by applying high heating rates ($S_h \geq 40$ °C/min) the question still remains whether the extensive reorganization effects influencing the lowest melting peak can be hindered by high heating rates. As is seen, T_{m1} and T_m follow the crystallization temperature with increasing cooling rate only partly indicating that extensive reorganization still takes place during heating. Thus, though it is evident that the higher the heating rate, the more the reorganization is hindered, obviously, a much higher heating rate is needed to fully prevent these reorganization effects for PP, and by that to (re)connect the melting with the crystallization behavior.

3.2. Polyoxymethylene (POM)

3.2.1. Introduction

Polyoxymethylene is a polymer with a well-known thermal behavior, which has been studied extensively. Relevant information concerning molecular structure, processing, crystallization, melting and resulting morphology can be found in several papers and textbooks [23–27].

Polyoxymethylene, also known as acetal resin, polytrioxane, polyformaldehyde, and paraformaldehyde, is an engineering plastic used to make gears, bushings and other mechanical parts. It is sold under the trade names Delrin®, Celcon®, and Ultraform®, the last two being copolymers. Its chemical formula is $-(-O-CH_2-)_n-$.

To make a polyoxymethylene homopolymer, anhydrous formaldehyde must be generated. The principal method is by reaction of aqueous formaldehyde with an alcohol to create a hemiformal, dehydration of the hemiformal/water mixture (either by extraction or vacuum distillation) and release of the formaldehyde by heating the hemiformal. The formaldehyde is then polymerized by anionic catalysis while the resulting polymer is stabilized by reaction with acetic anhydride.

To make a polyoxymethylene copolymer, formaldehyde is generally converted to trioxane. This is done by acid catalysis (either sulfuric acid or acidic ion exchange resins) and concurrent removal of the trioxane by distillation or extraction. The trioxane is then dried to remove all water and other active hydrogen containing impurities.

The comonomer is typically dioxolane but ethylene oxide can also be used. Dioxolane is formed by reaction of ethylene glycol with a formaldehyde source (trioxane or concentrated aqueous formaldehyde) over an acid catalyst. Other diols can also be used.

The stable polymer is melt compounded, adding thermal and oxidative stabilizers and optionally lubricants and miscellaneous fillers.

Automotive applications of acetal homopolymer resins include fuel-system and seat-belt components, steering columns, window-support brackets, and handles. Typical plumbing applications that have replaced brass or zinc components are shower heads, faucet cartridges, and various fittings. Consumer items include quality toys, garden sprayers, stereo cassette parts, butane lighter bodies, zippers, and telephone components. Industrial applications of acetal homopolymer include couplings, pump impellers, conveyor plates, gears, sprockets, and springs.

Industrial and automotive applications of acetal copolymer include gears, cams, bushings, clips, lugs, door handles, window cranks, housings, and seat-belt components. Plumbing products such as valves, valve stems, pumps, faucets, and impellers utilize the lubricity and corrosion and hot-water resistance of the copolymer. Mechanical components that require dimensional stability, such as watch gears, conveyor links, aerosols, and mechanical pen and pencil parts, are other uses. Parts that require improved load-bearing stability at elevated temperatures, such as cams, gears, TV tuner arms, and automotive underhood components are molded from glass-fiber-reinforced grades.

3.2.2. Results and discussion

Neat POM and POM's containing various amounts of stabilizer – 1.4, 3.4, 4.5 and 5.4 mass% of dioxalane – which latter "POM-modified samples" were obtained after several recrystallization cycles in solution, have been characterized by HPer DSC. The melting and crystallization behavior of the samples were investigated using various cooling and heating rates. The heat flow rates of neat POM and of a POM-modified sample containing 5.4 mass% of dioxalane cooled at rates varying from 5 to 300 °C/min are plotted as a function of the temperature in Fig. 6a and b. The curves, and by that the onset and peak temperatures, shift towards lower temperatures with increasing cooling rates as expected. The sample mass has been kept low, in between 0.4 and 0.7 mg, because the subsequent heating rate was 150 °C/min (the resulting heating curves are presented in Fig 8). For such low sample masses all cooling curves show a good quality (signal-to-noise ratio), even those measured at low rates like for $S_c = 5$ and 10 °C/min, which reflects the good performance of the HPer DSC used. When – like in the present case – a sample is exposed to manifold temperature–time ramps, consisting of various cooling and heating rates without refreshing in between, it has to be checked whether possibly degradation of the sample occurred. This is done by performing and comparing measurements in duplicate and by deciding whether the deviation(s) found – if there are any – are acceptable. For the measurements in Fig. 6a and b the check has been performed by programming the last measurement in duplicate of the first one by cooling at 150 °C/min, and the deviation seen was judged to be acceptable.

At first sight, there is only one crystallization exotherm present in the cooling curves. However, when the cooling rate is increased, in addition a second, small exotherm is observed at lower temperatures, which shifts from approximately 90 °C to approximately 80 °C. This intriguing small crystallization peak has not been ascribed in literature yet, but an analogous

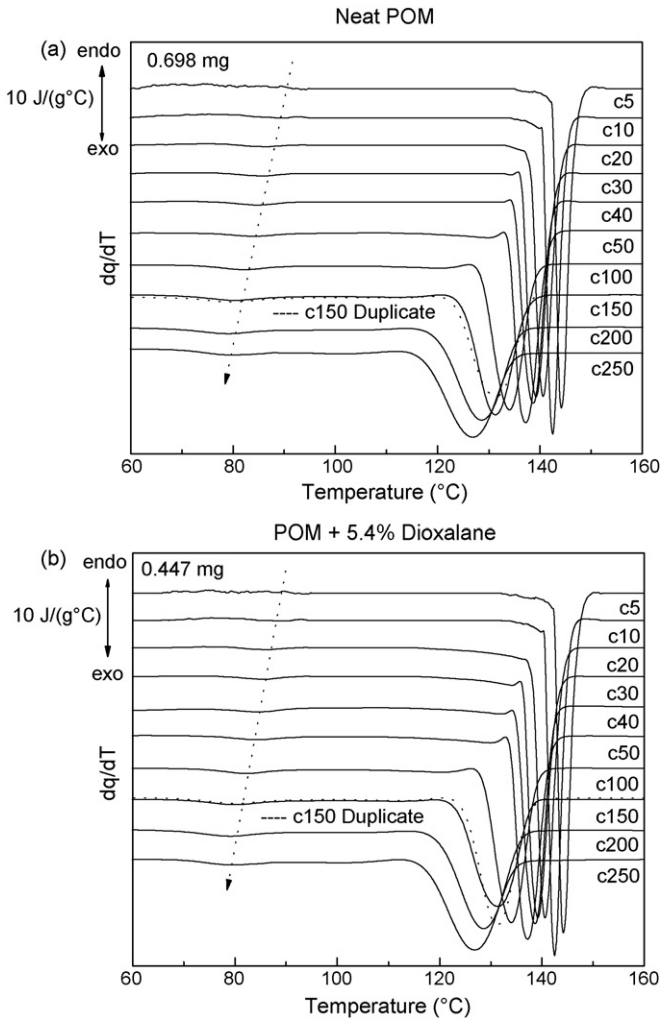

Fig. 6. HPer DSC cooling curves at various cooling rates of (a) neat POM and (b) POM modified with 5.4 mass% dioxalane.

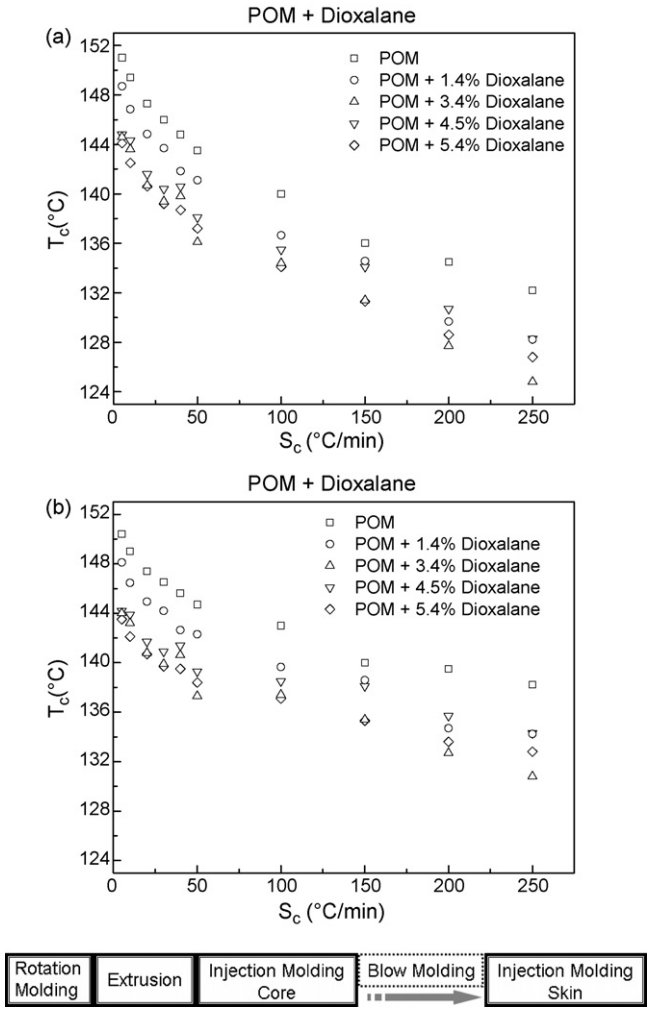

Fig. 7. Crystallization peak temperatures of neat POM and POM samples containing 1.4, 3.4, 4.5 and 5.4 mass% of dioxalane, as a function of the cooling rate: (a) uncorrected values and (b) values corrected for cooling rate and the sample mass.

phenomenon has been seen in almost all ethylene-based polymers, see e.g. Fig. 5.6 in [9].

Fig. 7 represents the crystallization peak temperatures as a function of the cooling rate of neat POM and of POM-modified samples containing respectively 1.4, 3.4, 4.5 and 5.4 mass% of dioxalane. For all cooling rates measured, the crystallization temperature decreases when the stabilizer content increases, meaning that the stabilizer disturbs the polymer chain while crystallizing: it behaves like a comonomer excluded from the crystallites. At zero and constant dioxalane content, similar to the crystallization behavior of PP, the crystallization temperatures of all samples decrease with increasing cooling rate. The uncorrected T_c values found for the POM and the POM-modified samples drop approximately 19 °C by changing the cooling rate from 5 to 250 °C/min (Fig. 7a). The *corrected* T_c values – corrections have been made for the sample mass and the cooling rate according to the procedure in Table IV of Ref. [2] – drop only 12 °C at increasing cooling rate from 5 to 250 °C/min (Fig. 7b). The drops of the crystallization temperatures are seen to be independent of the amount of dioxalane added. The characteristic crystallization temperatures, like the T_c values as measured here using HPer DSC, are very useful for industrial daily practice, because they mimic real crystallization temperatures under processing conditions like in case of rotation molding, extrusion, injection molding, etc.

The HPer DSC heating curves of the neat POM and of POM-modified samples, at a rate of 150 °C/min subsequent to cooling at various rates, show just one melting peak. For all samples, the melting peak temperature, T_m, values, see Fig. 8a, follow T_c to some extent only at low preceding cooling rates, which means that extensive reorganization still occurs like in the PP case. Similar to the crystallization behavior, the stabilizers in the POM-modified samples result in a general decrease of the melting temperatures compared with neat POM. The melting peak temperature depressions are even much stronger than the crystallization peak temperature depressions, approximately double figures are found when comparing Figs. 7b and 8a. In Fig. 8b the experimental results – corrected for 150 °C/min by a constant downward shift of 5 °C – can be fitted linearly when plotted on a logarithmic scale. The more stabilizer is added the lower are the slopes of the straight lines.

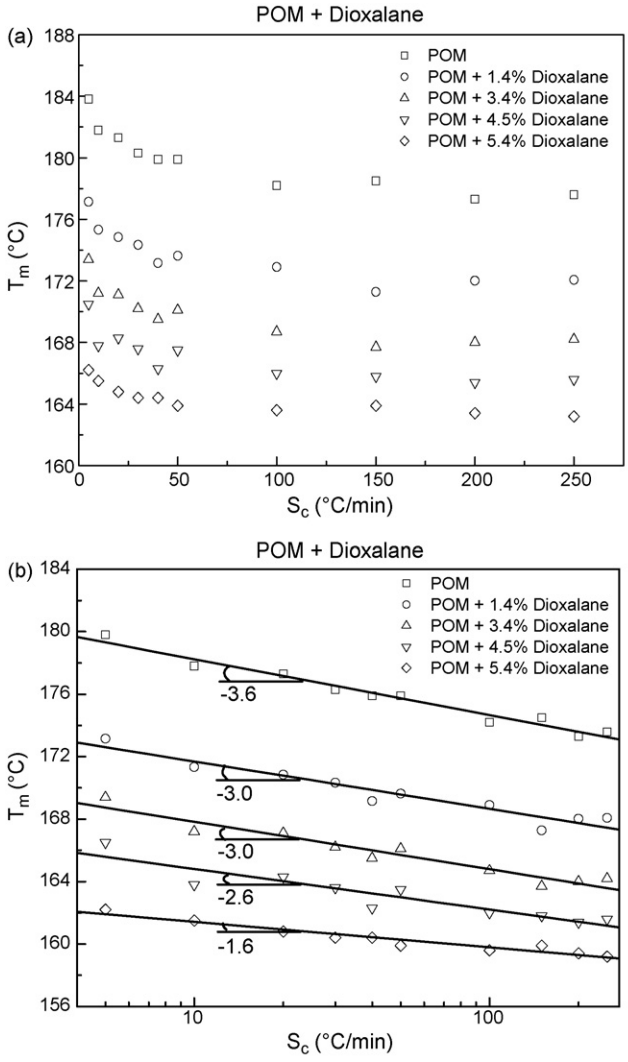

Fig. 8. Melting peak temperatures of neat POM and POM samples containing 1.4, 3.4, 4.5 and 5.4 mass% of dioxalane at a heating rate of 150 °C/min after various cooling rates (from 5 to 300 °C/min): (a) uncorrected data and (b) data (on a logarithmic scale) corrected for the heating rate; the sample mass has been kept constant at 1 mg.

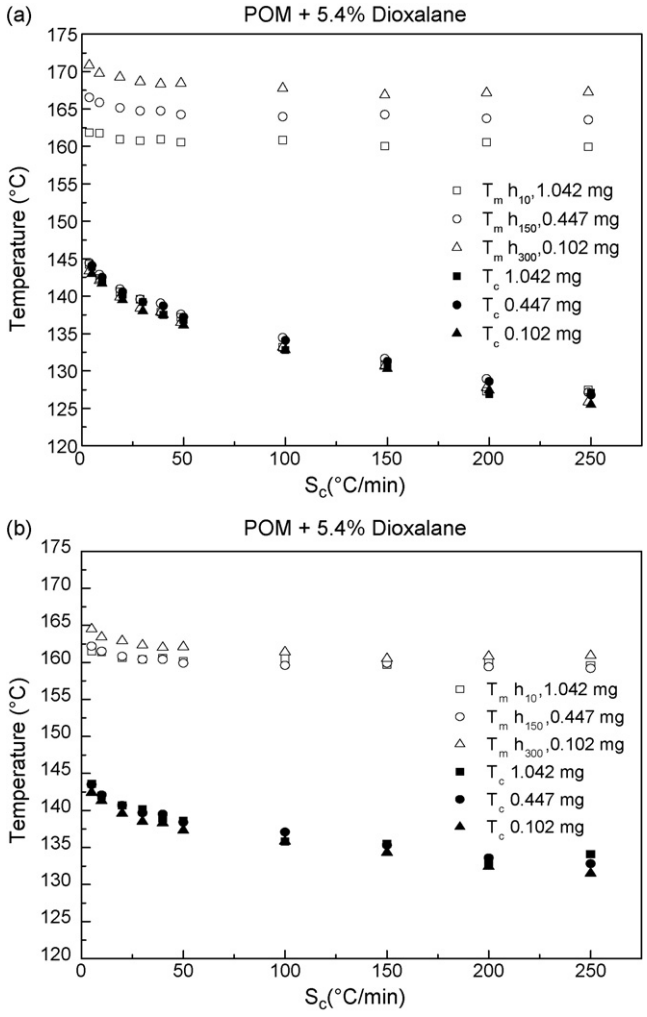

Fig. 9. Melting peak temperatures of a POM sample containing 5.4 mass% of dioxalane at heating rates of 10, 150 and 300 °C/min after various cooling rates (from 5 to 250 °C/min): (a) uncorrected and (b) corrected for heating rate and sample mass.

The uncorrected melting peak temperatures as obtained by HPer DSC measurements on the POM sample containing 5.4 mass% of stabilizer at heating rates of 10, 150 and 300 °C/min after different cooling rates (from 5 up to 250 °C/min) are shown in Fig. 9a. The T_m values show a dependency on the applied heating rate: faster heating leads to higher T_m values, as result of the thermal lag originated by the thermal resistance within the sample, the instrument and the thermal contact between sample container (aluminum foil) and instrument.

Fig. 9b shows the crystallization and melting peak temperatures resulting after correction for the applied cooling and heating rates respectively, and for their sample masses. Use has been made of the indium temperature calibration matrix previously determined (Table IV in Ref. [2]). After correction for the thermal lags, the T_m values almost coincide, though the T_m values of the sample heated at 300 °C/min are systematically located slightly above those of the samples heated at 10 and 150 °C/min (especially for low preceding cooling rates). This result seems to indicate that at high rates superheating takes place [35]. The T_c values (corrected for the cooling rate and sample mass) also come close to each other.

The appreciable corrections seen by comparing Fig. 9a and b show the importance of proper temperature calibration, and the necessity to arrive at a correct interpretation of thermal analysis data obtained at a variety of cooling rates, heating rates and sample masses. Of course this is crucial while HPer DSC becomes an indispensable analysis technique in industry in order to study polymer materials under processing conditions.

Self-seeding experiments have been performed to chart the boundaries for crystallization from the melt at high rates for both neat POM and the POM-modified sample with 5.4 mass% dioxalane. The self-seeding experiment starts with erasing the thermal history of the semicrystalline polymer by keeping it for 3 min at 200 °C, after which the sample is cooled at a rate of 150 °C/min to a temperature of 0 °C, followed by heating the sample at 150 °C/min towards a so-called “maximum temperature in the melt”, T_s, where it is hold for 3 min Then the sample

is cooled again at 150 °C/min towards 0 °C and reheated into the melt (up to 200 °C) where the sample stays again 3 min to erase the thermal history. Subsequently, the maximum heating temperature, T_s, is lowered by successive steps through the (isotropic) melting region of the semicrystalline polymer. Three different domains can be assigned to three different temperature intervals:

- Domain I is the (high) temperature interval where the thermal history is effectively erased and complete melting is realized.
- Domain II or "the self-seeding region" is the (intermediate) temperature interval where T_s is high enough to melt the material almost completely, but low enough to leave tiny crystal remains capable of acting as nuclei.
- Domain III is the (low) temperature interval where T_s is that low that only part of the crystals formed earlier is able to melt, which gives rise to both self-seeding by and annealing of the remaining crystals.

In literature self-seeding (or self-nucleation) is already mentioned by Blundell et al. [28], where the authors conclude that crystallization can be effectively influenced by self-seeding. The seeding technique not only reveals the existence of reminiscent nuclei but also enables the extension of crystallization studies to higher temperatures than before. Self-seeding increases the nucleation density, present in the sample as resulting from polymerization and possible subsequent processing, to a great extent by heating up the material within the self-seeding temperature interval (domain II or III) where crystal residues are capable to act as nuclei in subsequent cooling, which results in crystallization temperatures higher than without self-seeding (as would be the case after cooling from domain I). The influence of the maximum heating temperature in the melt on crystallization by DSC for various polyamides (PA6, PA6.6 and PA4.6) has been investigated by Mathot [29]. Under chosen conditions, the crystallization start- and peak temperatures increased when changing the highest temperature in the melt prior to cooling: up to about 30 °C above the normal end melting temperature, the crystallization behavior of polyamide 6 was influenced by the maximum temperature in the melt chosen. For polyamide 6.6 this was about 15 °C, and for polyamide 4.6 a few degrees. Extensive self-seeding experiments on polymer melts have been performed by Fillon et al. [30–32] using dynamic DSC.

The application of high heating and cooling rates with HPer DSC is very rewarding for performing self-seeding experiments because the measuring time and especially the time spent in the melt region is shortened, by which thermal degradation, chemical reactions in the melt, etc., are avoided or at least delayed. Therefore, using HPer DSC for the study of polymers properties as related to the temperature/time in the melt offers an advantage over Standard DSC.

Fig. 10 represents the melting peak temperatures: $T_{m,POM}$ and $T_{m,last,POM}$; $T_{m,5.4\%}$ and $T_{m,last,5.4\%}$; and the crystallization peak temperatures: $T_{c1,POM}$, $T_{c2,POM}$, $T_{c1,last,POM}$ and $T_{c2,last,POM}$; $T_{c1,5.4\%}$, $T_{c2,5.4\%}$, $T_{c1,last,5.4\%}$, $T_{c2,last,5.4\%}$, where "POM" and the index "5.4%" reflects the neat POM and the POM-modified sample with 5.4 mass% dioxalane, respectively. The indices 1 and 2 reflect the high-temperature crystallization peak temperature and the minor low-temperature crystallization peak temperature, respectively. The index "last" reflects the repetition of the first experiment, which is performed after all other experiments. All melting and crystallization temperatures of the POM-modified sample with 5.4 mass% dioxalane are 5–10 °C lower than those of the neat POM, which is expected regarding Figs. 6 and 8. For POM, by lowering the maximum temperature in the melt, T_s, prior to cooling, it is seen that T_{c1} increases for $T_s = 180$ °C, which is concluded to be the start of self-seeding according to domain I. For POM-modified with 5.4 mass% dioxalane, T_{c1}, domain I is situated below $T_s = 166$ °C. Domain III starts for neat POM at $T_s = 170$ °C for POM and for POM-modified with 5.4 mass% dioxalane at $T_s = 158$ °C.

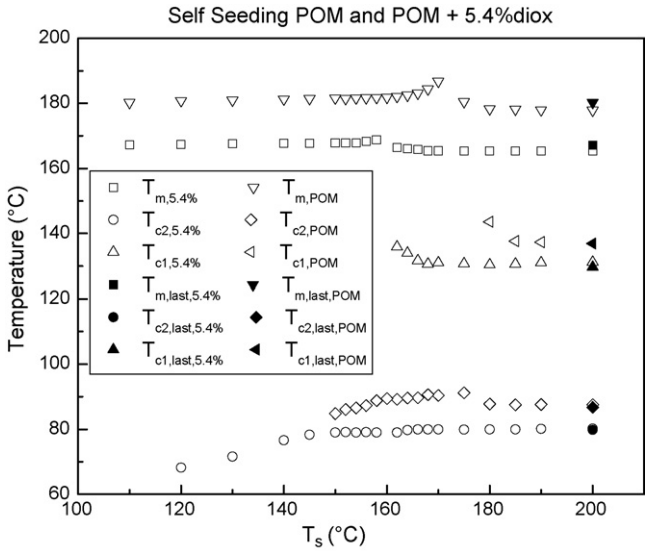

Fig. 10. The melting peak temperatures: $T_{m,POM}$ and $T_{m,last,POM}$; $T_{m,5.4\%}$ and $T_{m,last,5.4\%}$; and the crystallization peak temperatures: $T_{c1,POM}$, $T_{c2,POM}$, $T_{c1,last,POM}$ and $T_{c2,last,POM}$; $T_{c1,5.4\%}$, $T_{c2,5.4\%}$, $T_{c1,last,5.4\%}$, $T_{c2,last,5.4\%}$, where "POM" and the index "5.4%" reflects the neat POM and the POM-modified sample with 5.4 mass% dioxalane, respectively. The indices 1 and 2 reflect the high-temperature crystallization peak temperature and the minor low-temperature crystallization peak temperature, respectively. The index "last" reflects the repetition of the first experiment, which is performed after all other experiments.

It is remarkable that for both samples the minor low-temperature crystallization peak temperature T_{c2} is not influenced by the self-seeding behavior of the first, highest crystallization peak temperature: T_{c2} is still present and remains even constant when the highest temperatures in the melt are taken so low that T_{c1} already has been vanished. After a T_s of respectively 160 °C for POM and 150 °C for POM-modified with 5.4 mass% dioxalane the minor low-temperature crystallization peak temperature T_{c2} suddenly decreases. As the origin of this minor peak is not clear at all, no attention has been paid to explain this behavior.

The curves resulting from the measurements coded with "last" are hardly different from those from the first experiments, though the melting peak temperatures from the "last" experiments, $T_{m,last,POM}$ and $T_{m,last,5.4\%}$ are slightly (approximately 2 °C) increased with respect to $T_{m,POM}$ and $T_{m,5.4\%}$, respectively. To explore this phenomenon further, the POM-modified

sample with 5.4 mass% dioxalane has been studied according to its thermal stability. The sample has been heated and cooled at a rate of 100 °C/min repeatedly (11 times) in between −150 and 220 °C (higher than for the self-seeding experiments: 200 °C) with isothermal stays of 5 min (longer than for the self-seeding experiments: 3 min). These extreme cycling conditions result in an increase of the melting peak temperature, $T_{m,5.4\%}$, from 163.6 to 168.0 °C. This 4 °C increase is well in line with the increase of approximately 2 °C seen in Fig. 10, and can be explained by the occurrence of post-condensation.

3.3. Polyamide-6 (PA6)

3.3.1. Introduction

The many crystal structures for PA6 as reported in literature illustrate the complexity of the topic, all the more while the findings are often quite contradictory. The thermal behavior of PA6 is correspondingly much more complex compared to PP and POM. Because of new findings in this area are of crucial importance, in this introduction the present situation is discussed in some detail.

Studying the cooling behavior of PA6 is of importance because of the possible development of different crystal structures during cooling. The *monoclinic α structure* is well characterized and constitutes the major crystal fraction in PA6 samples when cooled in a standard way, like at 10 °C/min, or slower. It is a stable structure with a relatively high density of 1.235 g/cm^3 [33,34]. The melting enthalpy of 100 % crystalline PA having the α phase is calculated as 230 J/g [35,10] with a melting peak temperature in practice around 223 °C and an equilibrium melting point of 260 °C. The γ phase is also well characterized and is obtained by a KI/I_2 water solution treatment of α crystals [36–40]. The equilibrium melting temperature of this form is determined to be 214 °C, at a density of 1.190 g/cm^3 [39,41,42]. Illers [33] calculated a $\Delta H_{100\%}$ value of 239 J/g, which value is however affected by the density assumed (a $\Delta H_{100\%}$ value of 175 J/g has been found for a crystal density of 1.163 g/cm^3 [37]). In addition, several authors have proposed a third form, β, mostly obtained after fast quenching or cold crystallization of PA6 [34,43–45]. The precise characterization of this structure is heavily disputed, because the WAXD profile is very similar to the one of the γ form. Mostly, a *mesomorphic*, (*pseudo*)*hexagonal structure* is proposed [45], which is very unstable compared to the stable γ form obtained via the aqueous KI/I_2 treatment of α crystals, while it will give the α structure upon annealing. Various authors, however, have come up with different structures such as paracrystalline monoclinic α [44], pseudohexagonal γ* [33,39], pleated α [46], leading to a confusing nomenclature. Another group of authors states that the various structures found are nothing more than α or γ ones with various degrees of perfection, which structures can be viewed as intermediates between the two stable forms with respect to the H-bond setting and chain conformation [47–49]. Murthy [49] propose a disordered metastable phase and show that the stable γ form can be reversibly transformed into the metastable form under shear. Penel-Pierron et al. [50] summarize that while WAXD is not able to distinguish the γ form from the unstable mesomorphic β form (thus not indicating crystallographic dissimilarity), FTIR studies have indicated that the mesomorphic β form is closely related to the amorphous component from the standpoint of chain conformation. Thus, infrared spectroscopy was hardly able to separate the β mesomorphic contribution from the contribution of the amorphous phase [51]. FTIR, however, is able to discriminate between γ and β structures [52]. Illers [33] proposed a $\Delta H_{100\%}$ value of 60 J/g of the unstable form, labeled γ*, based on the specific volume (0.871 cm^3/g). Characteristic properties of the α- and γ-forms of PA6 can be found in the literature [33,34,38,39,44,49,53–62]. The heats of fusion at the equilibrium melting temperature, ΔH_f°, are the values reported by Illers [33]. Other values are reported in the literature [33,56,60,63–67] and Wunderlich has suggested a value of 230 J/g based on a compromise of various reports in the literature [35,10].

The effect of crystallization temperature and time on the formation of the α- versus γ-forms has been widely studied. Three independent investigations [59,68,69] have shown that crystallization for extended periods of time below ∼130 °C leads solely to the γ-crystallites while above ∼190 °C only the α-form is produced. Temperatures in between these limits result in a mixture of the two forms, with a higher fraction of α resulting the higher the temperature. Crystallization of PA6 at low temperatures, without the need of quenching, can be realized by fractionated crystallization [70–74]. Thus, the hypothesis mentioned for crystallization at low temperatures (γ-forms) could be checked by wide angle X-ray diffraction (WAXD).

Aliphatic polyamides show the so-called Brill transition in a high temperature region below the melting point, which was first observed in polyamide 6.6 [75]. This transition regards the merging of the two reflections of the α-form, which can be observed in plots of X-ray diffraction intensity versus 2θ [42,76–78] as the sample is heated.

Kyotani and Mitsuhashi [69] found that very short crystallization times at either 100 or 200 °C lead to both crystalline forms, while longer crystallization times produced predominantly γ and α, respectively. Annealing affects the crystal structure. For example, annealing of quenched samples, or those crystallized between 100 and 150 °C, at 200 °C for extended times leads to the conversion of γ-type of crystals into α ones [69,79–81]. Similar annealing results were demonstrated by Gogolewski et al. [60] and Gurato et al. [68].

Thus, in general, rapid cooling and low temperature crystallization is thought to promote the γ-phase of PA6, while higher crystallization temperatures or slow cooling leads to the α-phase. Kyotani and Mitsuhashi [69] assign the different temperature-dependent crystallization rates found to the existence of the two phases; i.e. at temperatures below 130 °C the rate of formation of γ is faster, while above ∼190 °C the crystallization rate of α is faster, while at intermediate temperatures, the rates are comparable. The maximum crystallization rate of PA6 occurs at approximately 140 °C [82]. The temperature dependence of the crystallization rate above this maximum is dominated by the nucleation barrier towards crystallization, while below, the rate is dominated by the diffusion restrictions to chains with respect to their moving towards the crystal growth fronts, i.e.

by the polymer chain (im)mobility. Therefore, it may be postulated that conditions of limited polymer chain mobility favor the crystallization of the γ-phase of PA6.

In all cases the driving force towards crystallization [9] is increasing with the supercooling; it increases with decreasing temperature. Thus, this driving force is the crucial function in "hot" (from the melt or high temperature during cooling) crystallization and in "cold" (from the glass state or from low temperature during heating) crystallization, and it equals (though with opposite sign) the driving force of melting. In fact, the specific driving force is the specific free enthalpy or specific Gibbs energy reference differential function, $\Delta g(T)$, which is calculated from the specific heat capacity reference differential function $\Delta c_p(T) = c_{pa}(T) - c_{pc}(T)$, where $c_{pa}(T)$ and $c_{pc}(T)$ are the specific heat capacities for the extreme situations in which the polymer at hand can be: 100% amorphous and 100% crystalline, respectively. The derivation of the driving force for a polymer [9,83] on the basis of heat capacity measurements illustrates the importance of performing quantitative calorimetry.

The above summary of literature shows the complexity of the polymorphous structures of PA6, in almost all cases leading to mixtures of α- and γ-like phases of different order, strongly dependent on crystallization conditions, such as the cooling rate. Thus, the structure actually realized when PA6 is crystallized from the melt will be influenced by many parameters including thermal conditions, applied stress, shear rate, humidity, pressure, additives that are present, etc.

Subsequent to cooling, it is of great interest to understand and interpret DSC heating curves with respect to the behavior of the crystal structures present. This is especially important in the case of polymorphous PA6 for which cold crystallization and multiple melting are commonly observed in DSC heating curves. In literature, several hypotheses have been proposed to explain multiple melting peaks in PA6. Usually the occurrence of continuous recrystallization events during the DSC heating scan has been put forward as explanation, and alternatively, different crystalline structures associated with the particular melting endotherms have been suggested in dependence of the crystallization temperature. In contrast to polyolefins, where almost unlimited possibilities of changing the molecular architecture exist, for polyamides differences in molecular structure as responsible parameters have been of less importance up till now. In order to better understand melting behavior in terms of polymorphism, HPer DSC experiments are of great value because the dynamic character as caused by the metastability of the systems scrutinized, and the kinetics involved, necessitate a full analysis exploiting the capabilities of HPer DSC with respect to its broad spectrum of cooling and heating rates.

3.3.2. Results and discussion

In the same way as described above for PP and POM, the crystallization behavior with varying cooling rates of PA6 has been studied by HPer DSC (see Fig. 11b). As the cooling rate increases, the crystallization peaks shift towards lower temperatures as expected while the curves show appreciable broadening,

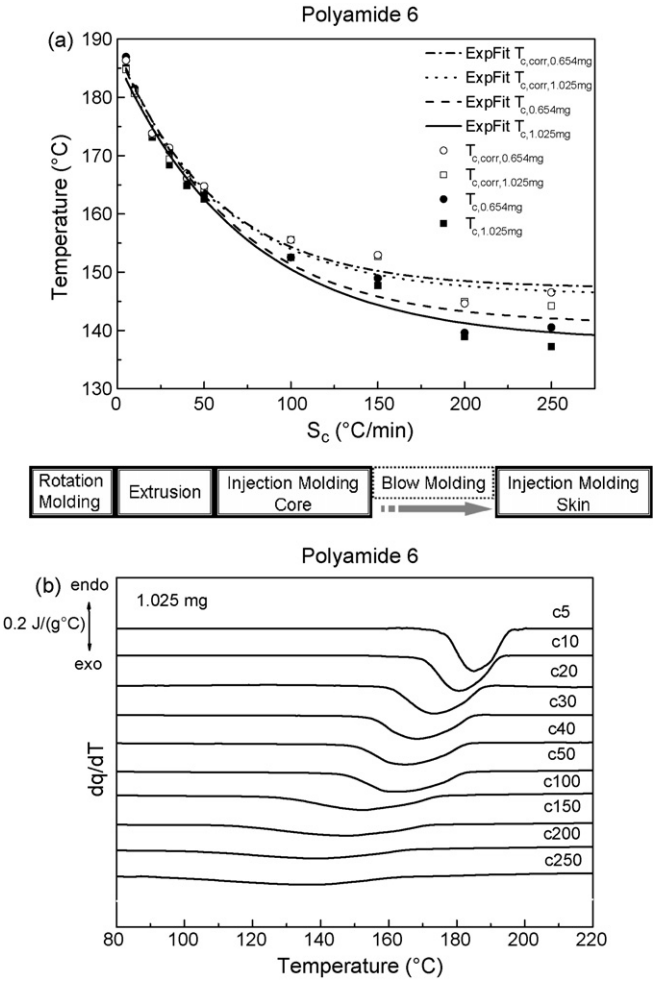

Fig. 11. (a) Crystallization peak temperature of PA6 samples having different masses as a function of cooling rate. (Filled symbols) T_c values without correction. (Open symbols) T_c values corrected for the sample mass and for the cooling rate applied. (b) Crystallization behavior of PA6 at various cooling rates.

as a result of which a crystallization peak temperature determination becomes almost impossible in case of the highest cooling rates.

Therefore, as will be obvious, defining a crystallization peak temperature for virgin (as received from provider) PA6 material might not always be as transparent as for PP and POM (which in addition have intrinsically higher heat flow rates), which phenomenon has been noticed already in the past. In addition, in practice, it turns out that the crystallization peak temperature of a curve may vary a few degrees centigrade between different samples. As a result, the spread concerning the data can be quite large in comparison with other polymers like PP and POM. Fig. 11a represents the crystallization peak temperatures of PA6 samples with two masses, 1.025 and 0.654 mg, for cooling rates, S_c, ranging from 5 to 250 °C/min. Corrections of the peak temperature values for sample mass and cooling rate have been made according to Table IV in Ref. [2], and as a result the T_c values are shifted to higher temperatures. On average, the drops in crystallization peak temperatures, as caused by increasing the cooling rate from 5 to 250 °C/min, amount to approximately 44 °C and approximately 37 °C for the uncorrected and

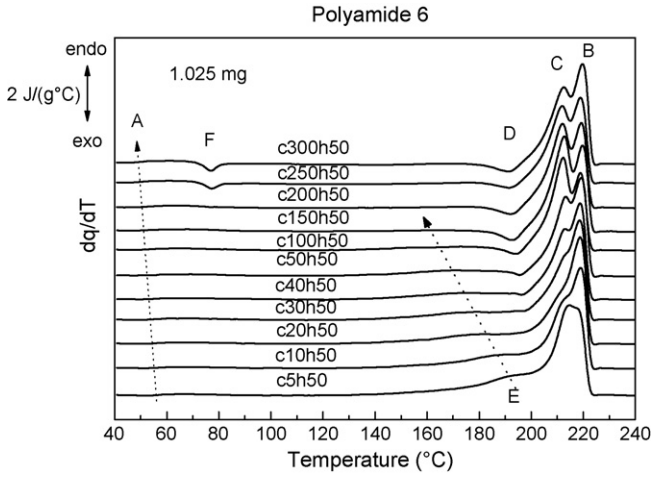

Fig. 12. Melting behavior of PA6 during heating at 50 °C/min subsequent to various preceding cooling rates.

corrected data, respectively. After correction, the crystallization peak temperatures are seen to come closer, as is also apparent from comparing the first-order exponential fitting curves for the two sample masses.

The melting behavior of PA6 as a function of the preceding cooling rate is shown in Fig. 12, and it is clearly observed to be much more complex than in case of PP and POM. The applied heating rate, 50 °C/min and the sample mass (1.025 mg), are kept the same for all measurements in order to compare the melting curves with the same correction. In the figure, several transitions (A–F) are indicated. These transitions change continuously with increasing cooling rates.

Between 50 and 60 °C (transition A) a glass transition range is observed, which is the characteristic for dry PA6. The glass transition in the heating curves is seen to shift towards lower temperatures with increasing cooling rates, which is unexpected: a higher cooling rate should induce a *higher* glass transition temperature. Because all curves have been measured at the same heating rate of 50 °C/min, this cannot be caused by thermal lag.

Three melting endotherms (transitions B, C and E) are detected. Each of them behaves different when the preceding cooling rate is increased: the melting endotherm E shifts drastically to lower temperatures, becomes broader, and then vanishes at the highest heating rates. Transition C shifts slightly to lower temperatures while transition B remains at the same temperature when increasing the preceding cooling rate. Increasing the preceding cooling rate from 30 °C/min to higher values, a small exotherm (transition D) appears just beneath 200 °C which shifts to 190 °C. Once the cooling rate is higher than 200 °C/min, cold crystallization around 75 °C is observed (transition F). Unexpected is the development of the heat flow rate ratio of peak denoted by C compared to peak denoted by B, "C/B)": from low to high preceding cooling rates, C/B decreases; increases and decreases again.

According to literature there are at least two possible explanations for the complex melting phenomena seen with varying preceding cooling rate: (1) the transitions are considered as being related to phase changes and (2) the transitions are thought to be caused by extensive reorganization effects like recrystallization and crystal thickening:

1. According to literature, it is "common knowledge" that the melting temperature of PA6 of the γ-phase is found around 214 °C and for the α-phase around 220 °C. The β-phase is mostly obtained after fast quenching or cold crystallization of PA6. Considering that slow cooling leads only to the α-phase, the endotherms C and B in curve c5h50 in Fig. 12 are ascribed to melting, and remelting after recrystallization of the α-phase. The small melting endotherm (transition E) around 190 °C is currently not well defined/described in literature, due to lack of instruments capable of cooling and heating rapidly like HPer DSC. Upon increasing the preceding cooling rate this endotherm shifts to lower temperatures following to some extent the descent of the crystallization peak temperature with increasing cooling rate. Therefore, it may be ascribed as reflecting a less perfect α-phase, which recrystallizes upon further heating resulting in the melting endotherms C and B. The higher the preceding cooling rate, the higher the peak of transition B is in comparison with the peak of transition C (curves c5h50–c20h50). This result can be understood because faster cooling results in less perfect α-crystals and these crystals start to reorganize/recrystallize earlier, which means more time to increase the stability of the crystals by perfectioning and increasing dimensions, and therefore more contribution to the higher melting peak. At a cooling rate of 30 °C/min suddenly an exotherm appears around 195 °C (transition D) which becomes more pronounced at higher cooling rates. Simultaneous with this appearance of the exotherm, the peak of transition C increases in comparison with the peak of transition B (curves c30h50–c150h50). Both phenomena are thought to be originated from γ-crystals. This explanation can be completed with the knowledge that rapid cooling and low temperature crystallization promotes the γ-phase of PA6. At the highest preceding cooling rates (the c250h50 and c300h50 curves) cold crystallization occurs around 75 °C (transition F) upon heating, which reflects the β-phase. Together with the appearance of cold crystallization the peak of transition B increases again in comparison with the peak of transition C, which is caused by reorganization of the β-phase into the α-phase on heating, resulting in an extra contribution to the melting endotherm B.
2. An alternative explanation is based on reorganization effects: melting, recrystallization, remelting and crystal thickening. Slow cooling leads to crystal structures with a variety of perfection, which is observed by the multiple endotherms upon heating (transitions E, C and B) where the last melting peak reflect the most perfect crystal structure after continuously reorganization and/or recrystallization. Higher cooling rates will accelerate crystallization at low temperatures, in general resulting in less perfect crystallites of small dimensions, which are vulnerable to reorganization upon heating. This explains early melting: transition E shifts to lower temperatures. Exotherm D may be present even at low cooling rates but is then probably masked by endotherm E. Exotherm D is speculatively ascribed to crystal thickening which is

favored by chain mobility at rather high temperatures and – for polyamides of less importance – on the chain microstructure. Whether such crystal thickening occurs will further depend on the actual crystalline structure in the sample. It remains unclear why exotherm D shifts. High cooling rates like presented by curves c200h50 and c300h50 lead to less crystallization/lower crystallinity of PA6. Part of the uncrystallized PA6, however, is able to cold crystallize on heating resulting in peak F. This low-temperature crystallized material will be very susceptible to continuous crystal perfection during heating what is reflected in an extra contribution to the peak B. The explanation of the ratio C/B cannot easily be found.

At first sight, using the different crystal phases (α, γ and β) in order to explain the melting behavior of PA6 as a function of the preceding cooling rate (explanation 1) looks quite logical. Nevertheless, the authors are somewhat skeptic and believe reality is more complicated than discussed above. Most probably, a combination of explanations (1) and (2) is operative.

It is important to realize that the crystallization and melting behavior, as revealed by DSC/HPer DSC, reflects molecular structure and morphology only indirectly. The length scales probed by techniques like time-resolved synchrotron small angle X-ray scattering and wide angle X-ray diffraction (SAXS/WAXD); and chain/segment/group mobilities as probed by solid-state NMR are of fundamental interest in understanding Standard DSC/HPer DSC heating curves in terms of morphology. Thus, to prove or disprove the abovementioned reasoning, additional morphological evidence has to be sought. Such a study will be the topic of a forthcoming paper.

4. Conclusions

The dynamics of crystallization and melting behavior, including the kinetics of reorganization and recrystallization have been studied for PP, POM and PA6, by means of varying sample masses, composition of the samples, cooling and heating rates. Corrections concerning thermal lag, when using different sample masses and/or high scan rates, are found to be necessary and have been applied and discussed. The influence of the cooling rate on the crystallization behavior has been studied and found to be of great help, not only for scientific purposes, but also for interpreting results of processing, and for mimicking realistic conditions of practice in general. It has been shown that cold crystallization, reorganization and recrystallization effects during heating at various rates can be studied successfully if performed in combination with a variety of preceding cooling rates. The use of high heating and cooling rates has finally been used to explore the dynamics of self-seeding.

Acknowledgement

This work was performed in the framework of a European Union Marie Curie Industry Host Fellowship of Dr. Geert Vanden Poel: contract no. HPMI-CT-2002-00180. All measurements were performed at DSM Research in The Netherlands. The POM samples were provided by Dr. Joachim Clauss from the Ticona Company, who is thanked for clarifying discussions. The authors also appreciate the discussions with Dr. Monika Basiura, SciTe/DSM Resolve, The Netherlands, and Mr. Peter Meijers of DSM Resolve, The Netherlands.

References

[1] T.F.J. Pijpers, V.B.F. Mathot, B. Goderis, R.L. Scherrenberg, E. van der Vegte, Macromolecules 32 (2002) 3601.
[2] G. Vanden Poel, V.B.F. Mathot, Thermochim. Acta 446 (2006) 41.
[3] V.B.F. Mathot, G. Vanden Poel, T.F.J. Pijpers, Am. Lab. 38 (14) (2006) 21 (See also a recent Webcast by V.B.F. Mathot, downloadable for free via www.scite.eu).
[4] S.C. Mraw, D.F. Naas, J. Chem. Thermodyn. 11 (1979) 567.
[5] Å. Fransson, G. Bäckström, Int. J. Thermophys. 6 (1985) 165.
[6] J. Karger-Kocsis, Polypropylene: An A–Z Reference, Kluwer Academic Publication, 1999.
[7] P. Edward, Moore Polypropylene Handbook: Polymerization, Characterization, Properties, Processing, Applications, Hanser-Gardner Publications, 1996.
[8] G. Harutun, Karian Handbook of Polypropylene and Polypropylene Composites, Marcel Dekker, 1999.
[9] V.B.F. Mathot, in: V.B.F. Mathot (Ed.), Calorimetry and Thermal Analysis of Polymers, Hanser Publishers, Munich, Germany, 1994, p. 105 (Chapter 5).
[10] M. Pyda (Ed.), ATHAS Data Bank, 1994. http://athas.prz.rzeszow.pl (for a description see: B. Wunderlich, Pure Appl. Chem. 67 (1995) 1019).
[11] F. De Santis, S. Adamovsky, G. Titomanlio, C. Schick, Macromolecules 39 (2006) 2562.
[12] N.E. Hager, Rev. Sci. Instrum. 35 (1964) 618.
[13] T.W. Kenny, P.L. Richards, Phys. Rev. Lett. 64 (1990) 2386.
[14] D.W. Denlinger, E.N. Abarra, K. Allen, P.W. Rooney, M.T. Messer, S.K. Watson, F. Hellman, Rev. Sci. Instrum. 65 (1994) 946.
[15] S.L. Lai, G. Ramanath, L.H. Allen, P. Infante, Appl. Phys. Lett. 70 (1997) 43.
[16] M. Zhang, M.Y. Efremov, F. Schiettekate, E.A. Olson, A.T. Kwan, S.L. Lai, T. Wisleder, J.E. Greene, L.H. Allen, Phys. Rev. B 62 (2000) 10548.
[17] M. Merzlyakow, C. Schick, Proc. NATAS (2000) 714.
[18] A.T. Kwan, M.Y. Efremov, E.A. Olson, F. Schiettekate, M. Zhang, P.H. Geil, L.H. Allen, J. Polym. Sci. B: Polym. Phys. 39 (2001) 1237.
[19] M. Zhang, M.Y. Efremov, E.A. Olson, Z.S. Zhang, L.H. Allen, Appl. Phys. Lett. 81 (2002) 3801.
[20] M. Merzlyakow, Thermochim. Acta 403 (2003) 65.
[21] S.A. Adamovsky, A.A. Minakov, C. Schick, Thermochim. Acta 403 (2003) 55.
[22] A.W. van Herwaarden, Thermochim. Acta 432 (2005) 192.
[23] K.H. Illers, Polym. Bull. 15 (1986) 265.
[24] P.D. Coates, A.G. Gibson, I.M. Ward, J. Mater. Sci. 15 (1980) 359.
[25] A.K. Taraiya, M.S. Mirza, J. Mohanraj, D.C. Barton, I.M. Ward, J. Appl. Polym. Sci. 88 (2003) 1268.
[26] B. Wunderlich (Ed.), Thermal Analysis of Polymeric Materials, Springer, Berlin.
[27] J. Mohanraj, D.C. Barton, I.M. Ward, A. Dahoun, J.M. Hiver, C. G'Sell, Polymer 47 (2006) 5852.
[28] D.J. Blundell, A. Keller, A.J. Kovacs, J. Polym. Sci. B: Polym. Lett. 4 (1966) 481.
[29] V.B.F. Mathot, Calorimetry and Thermal Analysis of Polymers, Hanser Publishers, Munich, Germany, 1994, p. 231 (Chapter 9).
[30] B. Fillon, J.C. Wittmann, B. Lotz, A. Thierry, J. Polym. Sci. B: Polym. Phys. 31 (1993) 1383.
[31] B. Fillon, B. Lotz, A. Thierry, J.C. Wittmann, J. Polym. Sci. B: Polym. Phys. 31 (1993) 1395.
[32] B. Fillon, A. Thierry, J.C. Wittmann, B. Lotz, J. Polym. Sci. B: Polym. Phys. 31 (1993) 1407.
[33] K.-H. Illers, Makromol. Chem. 179 (1978) 497.
[34] D.R. Holmes, C.W. Bunn, D.J. Smith, J. Polym. Sci. 17 (1955) 159.

[35] B. Wunderlich, Macromolecular Physics, vol. 3: Crystal Melting, Academic Press, New York, 1980.
[36] M. Tsuruta, S. Veda, T. Kiruma, Chem. High Polym. 15 (1958) 619.
[37] H. Arimoto, J. Polym. Sci. A 2 (1964) 2283.
[38] H. Arimoto, M. Ishibashi, M. Hirai, Y. Chatani, J. Polym. Sci. A 3 (1965) 317.
[39] K.-H. Illers, H. Haberkorn, P. Simák, Makromol. Chem. 158 (1972) 285.
[40] Y. Kinoshita, Makromol. Chem. 33 (1959) 1.
[41] P. Weigel, R. Hirte, C. Rusher, Faseforsch. Textiltech. 25 (198) (1974) 283.
[42] N.S. Murthy, S.M. Aharoni, A.B. Szollosi, J. Polym. Sci., Polym. Phys. Ed. 23 (1985) 2549.
[43] A. Ziabicki, Kolliod Z. 167 (2) (1959) 132.
[44] L.G. Roldan, H.S. Kaufmann, J. Polym. Sci., Polym. Lett. Ed. B 2 (1963) 603.
[45] F. Auriemma, V. Petraccone, L. Parravicini, P. Corradini, Macromolecules 30 (1997) 7554.
[46] R.F. Stepaniak, A. Garton, D.J. Carlsson, D.M. Wiles, J. Polym. Sci., Polym. Phys. Ed. 17 (1979) 987.
[47] J. Gianchandani, J.E. Spruiell, E.S. Clark, J. Appl. Polym. Sci. 27 (1982) 3527.
[48] J.P. Parker, P.H. Lindenmeyer, J. Appl. Polym. Sci. 21 (1977) 821.
[49] N.S. Murthy, Polym. Commun. 32 (10) (1991) 301.
[50] L. Penel-Pierron, C. Depecker, R. Séquéla, J.-M. Lefebvre, J. Polym. Sci. B: Polym. Phys. 39 (2001) 484.
[51] N.S. Murthy, R.G. Bray, S.T. Correale, R.A.F. Moore, Polymer 36 (20) (1995) 3863.
[52] G. Rotter, H. Ishida, J. Polym. Sci., Polym. Phys. 30 (1992) 489.
[53] S.M. Aharoni, *n*-Nylons, their Synthesis, Structure, and Properties, Wiley, Chichester, 1997.
[54] M.I. Kohen (Ed.), Nylon Plastics Handbook, Hanser, New York, 1995.
[55] F. Rybnikar, J. Burda, Faseforsch Textiltech 12 (1961) 324.
[56] T. Itoh, H. Miyaji, K. Asai, Jpn. J. Appl. Phys. 14 (2) (1975) 206.
[57] A. Reichle, A. Prietzschk, Angew. Chem. 74 (1962) 562.
[58] L.G. Walner, Monatsh 79 (1948) 279.
[59] K.H. Illers, H. Haberkorn, Makromol. Chem. 142 (1971) 31.
[60] S. Gogolewski, M. Gasiorek, K. Czerniawska, A.J. Pennings, Colloid Polym. Sci. 260 (9) (1982) 859.
[61] D.C. Vogelsong, J. Polym. Sci. A 1 (1963) 1055.
[62] T.D. Formes, D.R. Paul, Polymer 44 (2003) 3945.
[63] F. Rybnikar, Chem. Listy 52 (1958) 1042.
[64] P. Marx, C.W. Smith, A.E. Worthington, M. Dole, J. Phys. Chem. 59 (1955) 1015.
[65] M. Dole, B. Wunderlich, Makromol. Chem. 34 (1959) 29.
[66] M. Inoue, J. Polym. Sci. A 1 (1963) 2013.
[67] H.W. Starkweather Jr., P. Zoller, G.A. Jones, J. Polym. Sci., Polym. Phys. Ed. 22 (9) (1984) 1615.
[68] G. Gurato, A. Fichera, F.Z. Grandi, R. Zanetti, P. Canal, Makromol. Chem. 175 (3) (1974) 953.
[69] M. Kyotani, S. Mitsuhashi, J. Polym. Sci. A-2 10 (8) (1972) 1497.
[70] R.T. Tol, V.B.F. Mathot, G. Groeninckx, Polymer 46 (2005) 369.
[71] R.T. Tol, V.B.F. Mathot, G. Groeninckx, Polymer 46 (2005) 383.
[72] R.T. Tol, V.B.F. Mathot, G. Groeninckx, Polymer 46 (2005) 2955.
[73] R.T. Tol, V.B.F. Mathot, H. Reynaers, B. Goderis, G. Groeninckx, Polymer 46 (2005) 2966.
[74] R.T. Tol, A.A. Minakov, S.A. Adamovsky, V.B.F. Mathot, C. Schick, Polymer 47 (2006) 2172.
[75] R. Brill, J. Prakt. Chem. 161 (1942) 49.
[76] N.S. Murthy, S.A. Curran, S.M. Aharoni, H. Minor, Macromolecules 24 (11) (1991) 3215.
[77] C. Ramesh, E.B. Gowd, Macromolecules 34 (10) (2001) 3308.
[78] D.M. Lincoln, R.A. Vaia, Z.G. Wang, B.S. Hsiao, R. Krishnamoorti, Polymer.
[79] D.R. Salem, R.A.F. Moore, H.D. Weigmann, J. Polym. Sci. B: Polym. Phys. 25 (3) (1987) 567.
[80] I. Campoy, M.A. Gomez, C. Marco, Polymer 39 (25) (1998) 6279.
[81] A. Okada, M. Kawasumi, I. Tajima, T. Kurauchi, O. Kamigaito, J. Appl. Polym. Sci. 37 (5) (1989) 1363.
[82] J.H. Magill, Polymer 3 (1962) 655.
[83] V.B.F. Mathot, Polymer 25 (1984) 579 (Errata: V.B.F. Mathot, Polymer 27 (1986) 969).